

Chapter 6

Accelerator Systems Hardware

The RHIC Spin Accelerator project requires 48 helical dipole magnets placed in special arrangements within the RHIC accelerator lattice to produce necessary manipulations of the particle spin. To maintain polarization while crossing resonances, “Siberian Snakes” are required, which will consist of 4 helical dipoles in succession, each with right-handed helical fields that begin and end with the dipole field vertical. At the two major interaction points, spin “Rotators” will also be installed, which consist of 4 helical dipoles in succession, each with dipole fields that begin and end horizontally; however, these magnets will have alternating helicity – right-handed, left-handed, right-handed, left-handed. The helicity is given in order as seen by the beam. Fig. 1.2 shows schematically the layout of these devices. The Rotators are located at a warm-to-cold interface within the Q3-Q4 straight section. Thus, the orientation of the cryogenic piping dictates that there be two additional categories of Rotator, namely one which follows the warm-to-cold transition with a right-handed helix, and one which follows the warm-to-cold transition with a left-handed helix. Figs. 6.1 and 6.2 show Snake assemblies located between quadrupoles Q7 and Q8 in the 3 o’clock and 9 o’clock sections of RHIC, while Figs. 6.3 and 6.4 sketch out the Rotator locations near the major detectors.

Using these figures, we can summarize basic magnet requirements as shown in Table 6.1, and requirements for the completed assemblies in Table 6.2. Parameters and tolerances for magnets are given in Table 6.3. A complete list of devices, including their Site Wide Names (used in the RHIC lattice database and other lists) and their characteristics, is provided In Tables 6.4 and 6.5.

Magnet Model	Helicity	Field Orientation at Entrance and Exit	Quantity Required
HRCxxx	Right-handed	Vertical	16
HRDxxx	Right-handed	Horizontal	16
HRExxx	Left-handed	Horizontal	16

Table 6.1: Magnet quantities and types needed for Snakes and Rotators.

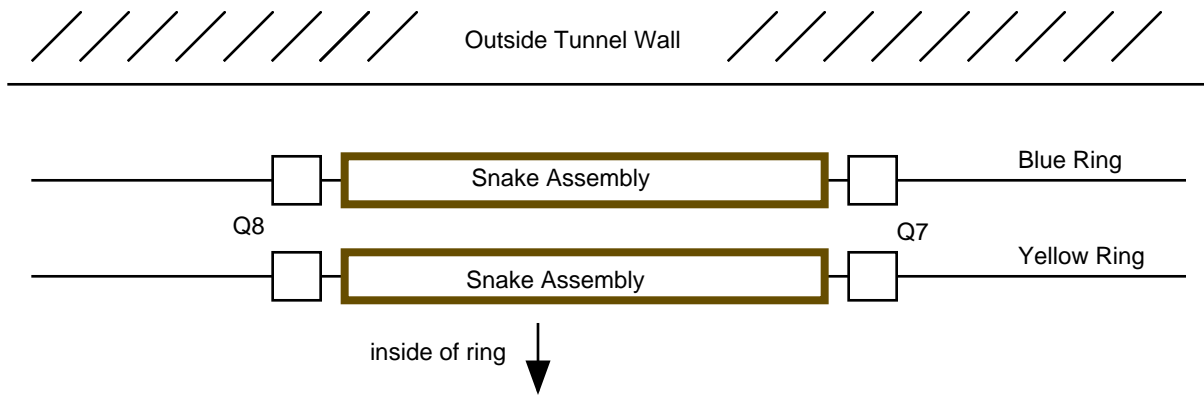


Figure 6.1: Schematic layout of Siberian Snake in the 3 o'clock Region of RHIC.

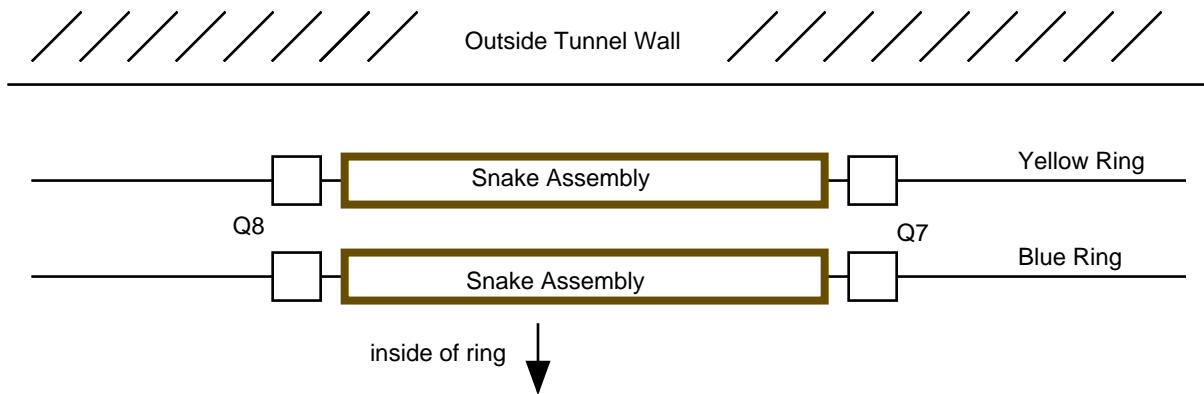


Figure 6.2: Schematic layout of Siberian Snake in the 9 o'clock Region of RHIC.

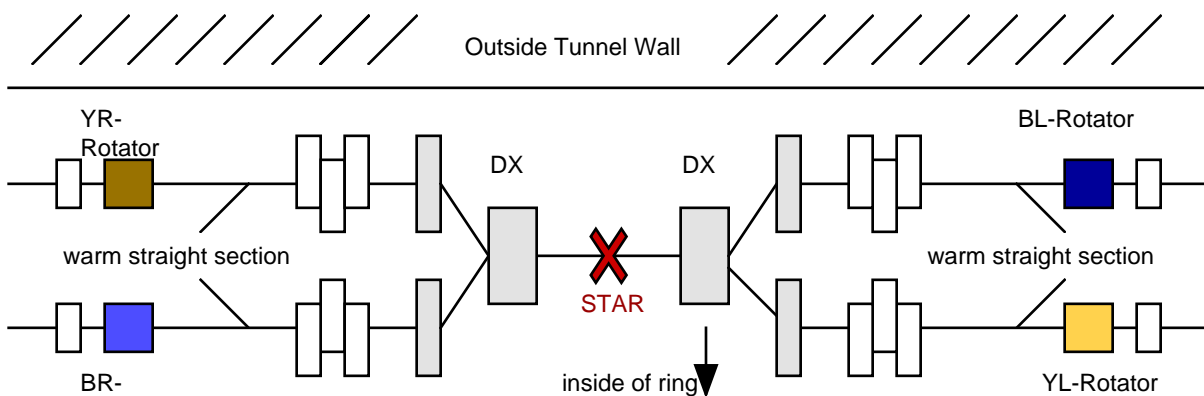


Figure 6.3: Schematic layout of Spin Rotators in the 6 o'clock Region of RHIC. The STAR detector is located at the interaction point. Further descriptions of the various Rotator units can be found in Table 6.2.

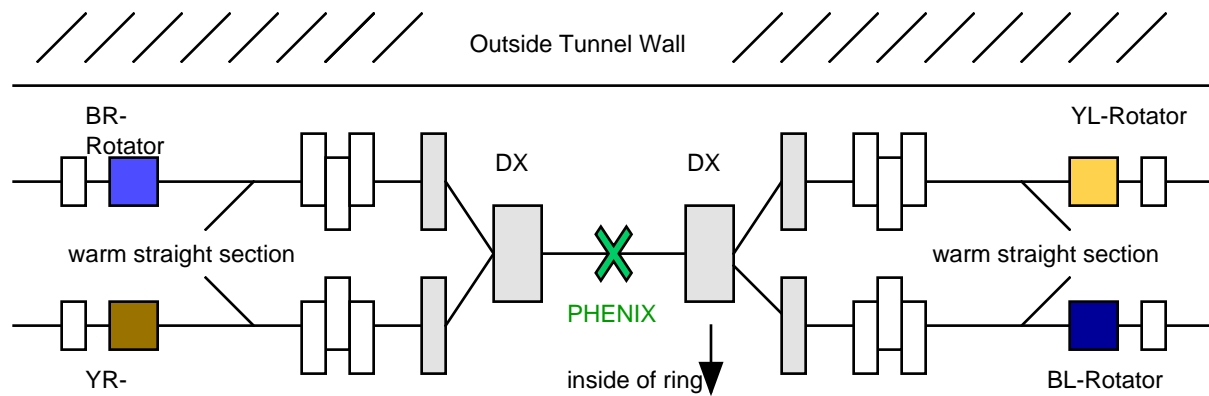


Figure 6.4: Schematic layout of Spin Rotators in the 8 o'clock Region of RHIC. The PHENIX detector is located at the interaction point. Further descriptions of the various Rotator units can be found in Table 6.2.

Unit Type	Field Orientation at Entrance/Exit	Helicity Pattern (*)	Quantity Required	W-to-C transition (**)	Unit Name
Snake	Vertical	RH,RH,RH,RH	4	(none)	(TBD)
Rotator (Blue/R)	Horizontal	RH,LH,RH,LH	2	RHS of unit	(TBD)
Rotator (Blue/L)	Horizontal	RH,LH,RH,LH	2	LHS of unit	(TBD)
Rotator (Yellow/R)	Horizontal	LH,RH,LH,RH	2	RHS of unit	(TBD)
Rotator (Yellow/L)	Horizontal	LH,RH,LH,RH	2	LHS of unit	(TBD)

Table 6.2: Quantities and types of complete Snake and Rotator assemblies. (*)The helicity pattern is the pattern seen if standing at the inside wall of the tunnel, looking radially outward. (**)The Warm-to-Cold transition occurs either on the right-hand-side of the unit or on the left-hand-side, as seen if standing at the inside wall of the tunnel, looking radially outward.

Parameter		Requirement	Tolerance (rms)
Design Central Field	B_0	4 Tesla	
Operating Margin		15 %	
Design Magnetic Length	$\frac{1}{B_0} \int B dL$	240 cm	
Magnet Slot Length		260.65 cm	
Total Cryostat Assembly Length		1186.815 cm	
Integrated Field Strength	$\int B dl$	9.6 Tesla-meter	0.05 T-m
Integrated Field Components	$\int B_x dl, \int B_y dl$	0 Gauss-m	500 Gauss-m
Quadrupole Coefficient of main dipole field	b_1	0	2.0
Sextupole Coefficient of main dipole field	b_2	2.0	2.0
Octupole Coefficient of main dipole field	b_3	0	2.0
Decapole Coefficient of main dipole field	b_4	2.0	1.0
Skew Quadrupole Coefficient of main dipole field	a_1	0	2.0
Transverse Alignment(*)	$\Delta x, \Delta y$	0 mm	0.5 mm
Longitudinal Alignment(*)	Δz	0 mm	1.0 cm
Rotational Alignment(*)	$\Delta \phi$	0 mrad	1.0 mrad

Table 6.3: General parameters and tolerances for an individual Snake or Rotator magnet. Magnet multipole coefficients are in units of 10^{-4} at 3.1 cm reference radius. (*)Alignment is with respect to neighboring quadrupoles.

Site Wide Name	Magnet Name	Type	Inside/ Outside	Sector	Location Number	Handedness	Field Orientation at End
bo3-snk7							
bo3-hlx7.4	HRCxxx	Sn	o	3	7	R	V
bo3-hlx7.3	HRCxxx	Sn	o	3	7	R	V
bo3-hlx7.2	HRCxxx	Sn	o	3	7	R	V
bo3-hlx7.1	HRCxxx	Sn	o	3	7	R	V
bi5-rot3							
bi5-hlx3.4	HRDxxx	Ro	i	5	3	R	H
bi5-hlx3.3	HRExxx	Ro	i	5	3	L	H
bi5-hlx3.2	HRDxxx	Ro	i	5	3	R	H
bi5-hlx3.1	HRExxx	Ro	i	5	3	L	H
bo6-rot3							
bo6-hlx3.1	HRDxxx	Ro	o	6	3	R	H
bo6-hlx3.2	HRExxx	Ro	o	6	3	L	H
bo6-hlx3.3	HRDxxx	Ro	o	6	3	R	H
bo6-hlx3.4	HRExxx	Ro	o	6	3	L	H
bo7-rot3							
bo7-hlx3.4	HRDxxx	Ro	o	7	3	R	H
bo7-hlx3.3	HRExxx	Ro	o	7	3	L	H
bo7-hlx3.2	HRDxxx	Ro	o	7	3	R	H
bo7-hlx3.1	HRExxx	Ro	o	7	3	L	H
bi8-rot3							
bi8-hlx3.1	HRDxxx	Ro	i	8	3	R	H
bi8-hlx3.2	HRExxx	Ro	i	8	3	L	H
bi8-hlx3.3	HRDxxx	Ro	i	8	3	R	H
bi8-hlx3.4	HRExxx	Ro	i	8	3	L	H
bi9-snk7							
bi9-hlx7.4	HRCxxx	Sn	i	9	7	R	V
bi9-hlx7.3	HRCxxx	Sn	i	9	7	R	V
bi9-hlx7.2	HRCxxx	Sn	i	9	7	R	V
bi9-hlx7.1	HRCxxx	Sn	i	9	7	R	V

Table 6.4: RHIC Spin helical dipole magnet locations – **BLUE Ring**.

Site Wide Name	Magnet Name	Type	Inside/ Outside	Sector	Location Number	Handedness	Field Orientation at End
yi3-snk7							
yi3-hlx7.4	HRCxxx	Sn	i	3	7	R	V
yi3-hlx7.3	HRCxxx	Sn	i	3	7	R	V
yi3-hlx7.2	HRCxxx	Sn	i	3	7	R	V
yi3-hlx7.1	HRCxxx	Sn	i	3	7	R	V
yo5-rot3							
yo5-hlx3.4	HRExxx	Ro	o	5	3	L	H
yo5-hlx3.3	HRDxxx	Ro	o	5	3	R	H
yo5-hlx3.2	HRExxx	Ro	o	5	3	L	H
yo5-hlx3.1	HRDxxx	Ro	o	5	3	R	H
yi6-rot3							
yi6-hlx3.1	HRExxx	Ro	i	6	3	L	H
yi6-hlx3.2	HRDxxx	Ro	i	6	3	R	H
yi6-hlx3.3	HRExxx	Ro	i	6	3	L	H
yi6-hlx3.4	HRDxxx	Ro	i	6	3	R	H
yi7-rot3							
yi7-hlx3.4	HRExxx	Ro	i	7	3	L	H
yi7-hlx3.3	HRDxxx	Ro	i	7	3	R	H
yi7-hlx3.2	HRExxx	Ro	i	7	3	L	H
yi7-hlx3.1	HRDxxx	Ro	i	7	3	R	H
yo8-rot3							
yo8-hlx3.1	HRExxx	Ro	o	8	3	L	H
yo8-hlx3.2	HRDxxx	Ro	o	8	3	R	H
yo8-hlx3.3	HRExxx	Ro	o	8	3	L	H
yo8-hlx3.4	HRDxxx	Ro	o	8	3	R	H
yo9-snk7							
yo9-hlx7.4	HRCxxx	Sn	o	9	7	R	V
yo9-hlx7.3	HRCxxx	Sn	o	9	7	R	V
yo9-hlx7.2	HRCxxx	Sn	o	9	7	R	V
yo9-hlx7.1	HRCxxx	Sn	o	9	7	R	V

Table 6.5: RHIC Spin helical dipole magnet locations – **YELLOW Ring**.

6.1 Helical Dipole Magnets

Two methods for building helical magnet coils have been pursued. The first, called the “slotted” coil method, is based upon established BNL technology used to produce the RHIC sextupole magnets. It consists of a Kapton-wrapped, round cable placed into helical grooves that have been milled into a thick-walled aluminum cylinder. Thin sheets of epoxy-loaded fiberglass are placed between layers, and the entire assembly is cured at elevated temperature and with radial pressure to produce a compact, strong matrix. A first prototype coil using this technique was built and tested at BNL, and a full field, half length prototype magnet was completed late in 1996. Testing showed this to be a sound design, and it has been chosen as the design for production. A full length magnet is being built in 1998 using a newly developed automatic winding machine.

A second method for coil production was studied, called the “direct-wind” coil method. This method consists of the same type of cable as the slotted design applied by machine directly to the surface of a stainless steel tube in multiple layers. The surface of the Kapton-wrapped cable has a coat of adhesive. A very thin layer of epoxy-loaded fiberglass is placed between layers. The cable is applied in a helical pattern by a computer-controlled multiple-axis winding machine. A full field, half length prototype magnet using this direct-wind method was built by AML, Inc., in Palm Bay, FL and tested at BNL. Testing indicated the need for some design changes to increase the mechanical stability of the conductor, particularly in the ends of the magnet, in order to reach the required field level with sufficient operating margin.

A firm requirement for the helical magnet is that it reliably reach a field of 4 T at an operating temperature of 4.6 K. To ensure this capability for all the magnets that may be built, a margin of at least 15% is prudent. This margin allows for normal variations in component quality and size, quality of assembly, and variation in operational conditions.

The design of the slotted coil helical magnet follows principles that are derived from the operation of any superconducting magnet: that high forces be contained, that superconductor motion (particularly stick/slip motion) be minimized, that energy be safely extracted from the magnet at quench, that the ends of the magnet be restrained, that cooling be adequate for the operational conditions, etc. A number of concepts developed in the SSC and RHIC magnet programs are used, in particular the construction method used for the coils of the RHIC sextupole magnet. The basic structure of the helical coil uses a new concept: helical slots milled into thick-walled aluminum cylinders to give a $\cos\theta$ current distribution in a two-dimensional section when the slots are filled with conductor. In the initial models the cylinders are wound by hand. This could be done without a large tooling expense but would be too labor intensive for more than a few models. For production, a wiring machine that can place the cable directly into the slots has been built, and is shown in Fig. 6.5. This machine uses the ultrasonic wire bonding technique developed for the automatic wiring machines used to build the corrector coils for the RHIC Project. Two of these cylinders, concentric with one another, are used to give the required field of 4 T. A cross section

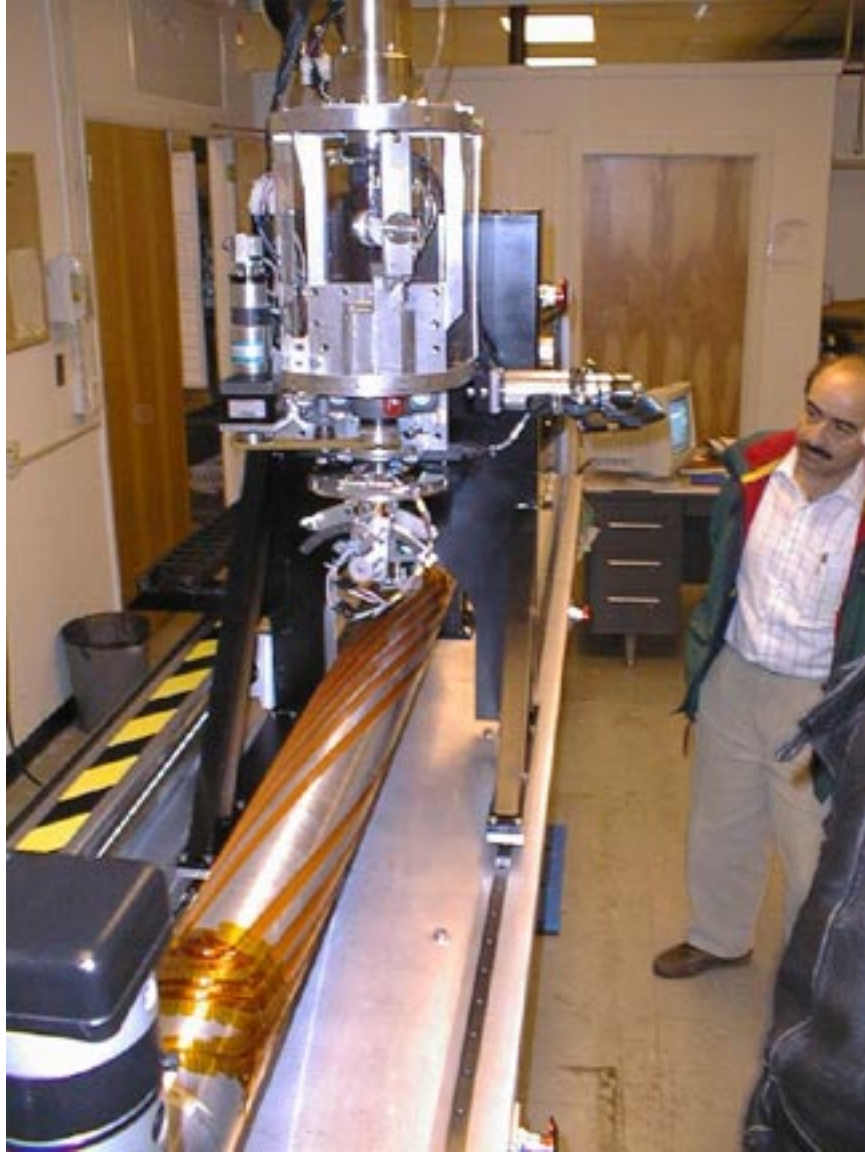


Figure 6.5: Automatic winding machine used for helical dipole coil production.

of the design is shown in Fig. 6.6.

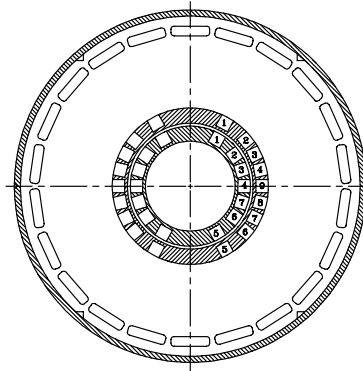


Figure 6.6: A cross section of the slotted coil helical magnet. The diameter of the iron yoke is 14 inches (355.6 mm).

The Lorentz forces are contained initially by the strength of the aluminum cylinders and the compressive force exerted by the overwrap of Kevlar and fiberglass/epoxy around the circumference of each coil. At high field, the cylinders distort into an elliptical shape, growing outward on the midplane. After deflecting outward a fraction of a millimeter, they reach the stop provided by the next tube or the iron yoke. These small elastic motions are not expected to affect the quench performance of the magnet nor to distort the field in any significant way.

A number of features have been incorporated into the design that would ensure that the 4 T requirement is satisfied. In addition to including a sufficient number of turns, the design was optimized for a higher current (11/9) in all but the pole blocks of the outer coil — this is possible because the field is lower in these places and the superconductor is able to carry more current before reaching its quench point. In most two-layer superconducting magnet designs, the conductor is graded so that more turns can be placed in the second layer; here the expense of developing a second conductor was avoided by increasing the current requirement in the second layer. Also, the iron yoke was designed to be close to the coil to increase the field in the magnet aperture. However, these various design features lead to harmonics in the magnet that are unduly large if the magnet is powered with only one current. If only one current is sufficient to reach the required field, then a layer of turns can be removed from each of the inner coil and outer coil pole current blocks to give suitably small harmonics.

The quench performance and harmonic content (given in units: parts/ 10^4 , at 31 mm radius) that were expected in the prototype magnet as built when operated with just one current, and no holes in the iron yoke, are given in Tables 6.6 through 6.9. Fig. 6.7 shows the current versus. field characteristic for the

prototype magnet, and for the superconductor that was used.

	$B_{ss}, T @ 4.35 \text{ K}$	$B_{ss}, T @ 4.6 \text{ K}$
Single current	5.0	4.55
Two currents	5.3	4.82

Table 6.6: Expected quench field (central field) in the prototype, slotted coil magnet, based on the short sample measurements made on the superconductor.

n	b_n (2-Dim)	b_n (Spiral)
2	-50.1	-2.9
4	5.4	0.73
6	0.4	-0.09
8	-7.5	0

Table 6.7: Expected values of the body harmonics for the one-current design. The “2-Dim” column gives the geometric harmonics assuming a straight coil, and the “Spiral” column gives the harmonics due to the spiral structure of the coils. Spiral harmonics have the x -dependence of the usual harmonic definition, but not the angular dependence — they have a dipole angular dependence.

n	b_n	a_n
2	0.2	164
4	0.04	19
6	0.04	3.8

Table 6.8: End harmonics in the lead plus return ends of the magnet, given in unit-meters.

6.1.1 Conductor

The conductor is a cable that is made up of seven strands of the 0.330 mm superconductor wire developed for the RHIC corrector program. This cable, nearly 1 mm in diameter, carries 314 A to produce a 4 T field in the present design. Using a cable in the magnet is preferable to using a single wire: if a break in a wire of that cable should occur, the magnet would very likely still operate satisfactorily. In addition, a cable is more flexible than an equivalent wire and therefore eases the manufacturing of the coils. The required Kapton insulation is wrapped onto the cable in the cable-manufacturing operation. The superconductor parameters are given in Table 6.10.

The cable is made with a 6-around-1 geometry, which results in a cable in which the center wire is not transposed along the length of the cable. Eddy currents are generated in this wire when the magnet

I , A	B_0 , T	$\delta(\text{TF})$, %	b_2	b_4	b_6	b_8
50	0.68	-0.1	-50.3	5.4	0.4	-7.5
90	1.23	-0.2	-50.6	5.4	0.4	-7.4
200	2.71	-0.6	-52.9	5.3	0.4	-7.5
300	3.87	-5.6	-71.4	1.8	0.3	-7.7
400	4.81	-11.9	-82.7	2.4	0.4	-8.3
500	5.71	-16.3	-84.5	4.0	0.5	-8.9

Table 6.9: Single current dependence of the field and 2-dimensional harmonics in the prototype magnet due to the saturation of the iron yoke. A current of 314 A is estimated to give a central field of 4 T. The geometric harmonics given in Table 6.7, which are valid at any current, must be subtracted from these to obtain the harmonic changes due to saturation.

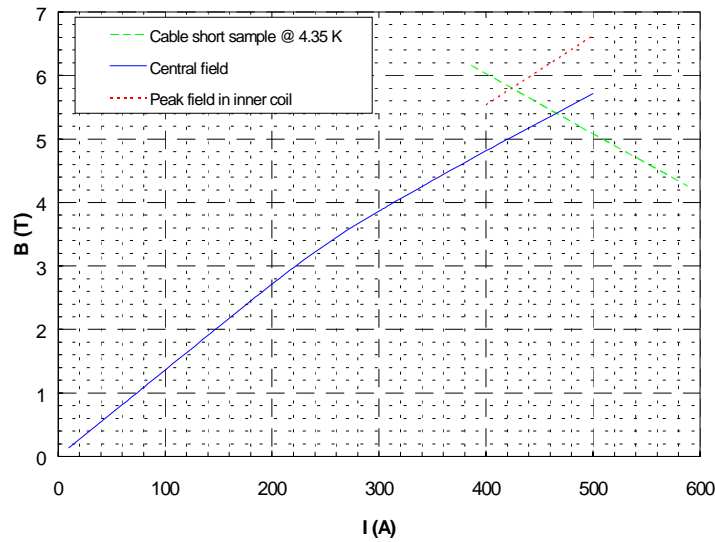


Figure 6.7: Field versus single current for the prototype slotted coil helical magnet. The central field is 4 T at 314 A. The peak field will determine the quench current, estimated at ~ 420 A.

	Parameter	Units	Value
Wire	Filament diameter	μm	10
	Filament spacing	μm	> 1
	Cu to non-Cu ratio		2.5:1
	Number of filaments		310 \pm 5
	Diameter, bare	mm	0.330
Cable	Min I_c @ 5 T, 4.2 K	A	68
	Number of Wires		7
	Cable style		6-around-1
	Diameter, bare	mm	0.991
	Diameter, insulated	mm	1.092
	Min I_c @ 5 T, 4.2 K	A	476

Table 6.10: Superconductor Parameters

current is ramped. These eddy currents generate heat and have a measurable effect on quench performance above a ramp rate of 2 A/s. Since these magnets are not required to ramp in operation, this design feature is not detrimental to the required performance.

The Kapton wrap on the cable allows space for helium inside the wrap, in direct contact with the wires. This is a desirable feature for enhancing the stability of the superconductor. It is estimated that there are somewhat over 10% voids for helium inside the Kapton wrap.

6.1.2 Mechanical Construction

The cable is laid in an ordered pattern into the Kapton-lined slots milled into the aluminum cylinders. A piece of fiberglass cloth impregnated with a B-stage epoxy is placed between each layer of wires in the slots. The slots continue around the ends in a layout designed to minimize undesired harmonics. When all the turns have been wound into the slots, G10 fiberglass pusher plates 3.18 mm thick are placed on top the turns. Then the assembly is temporarily compressed with Kevlar that is wrapped onto the cylinder under tension. The entire assembly is next placed into an oven for curing, thereby forming a series of current blocks around the cylinder in which each wire is firmly supported in a fiberglass/epoxy matrix. This design for supporting the cable turns is analogous to that developed for the wire turns in the RHIC sextupole magnet. After curing, any voids in the ends are filled with a mineral-loaded epoxy, a technique used in the SSC program for adding strength and rigidity to coil ends. A drawing of the inner coil is shown in Fig. 6.8.

The finished size of each cylinder is achieved by over-wrapping each cylinder with new Kevlar strand to compress the current blocks and then with bands of fiberglass/epoxy, followed by grinding to size after curing. The two cylinders are fitted into an iron yoke supported at one end by a plate that aligns the cylinders to a fixed position. Only a slight clearance exists between finished cylinders. The yoke is made up of one piece laminations having a ring of small holes on the outside perimeter. Tie-rods through these

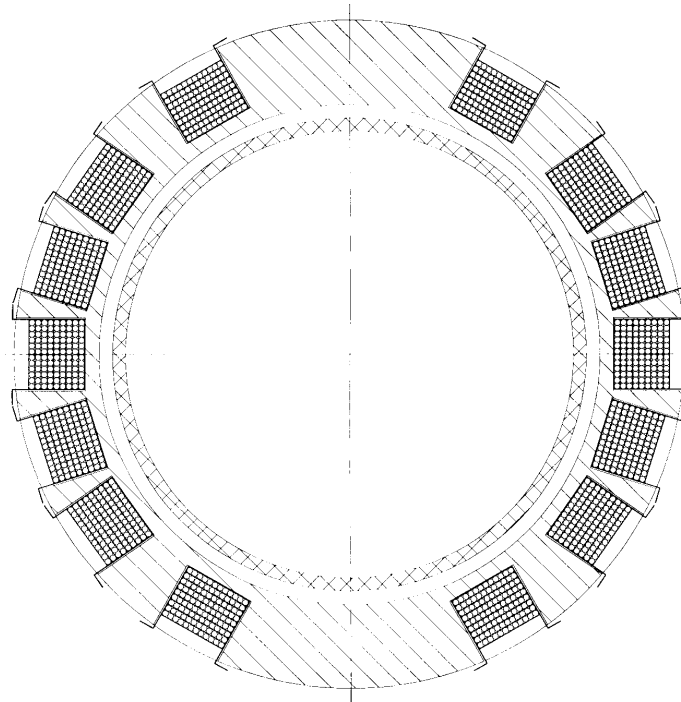


Figure 6.8: A detailed view of the inner coil of the slotted coil helical magnet. Each slot contains 108 turns of superconducting cable. The first layers of turns in the slots begin at a radius of 49.71 mm. The figure also shows the beam tube inside the coil.

holes in four places provide lateral restraint for the assembly (but are not required to restrain the axial Lorentz forces). Holes are also necessary for the passage of the helium coolant and the electrical buswork. The holes must be designed to minimize field irregularities as the field rotates along the length of the magnet. The inner radius of the yoke is increased in the ends to reduce the peak field on the conductor. A helium containment shell is welded in place around the yoke later when the entire unit is assembled into a complete helical Snake or Rotator.

This completed “storage unit” is now an independent, functional magnet, ready for installation into a cryostat (to be described later). The design at this point is similar to that of the arc CQS magnets for RHIC and the same concepts and methods from that construction are used as appropriate to complete the construction of the Snakes and Rotators. Mechanical parameters of the prototype storage unit are given in Table 6.11. Fig. 6.9 is a drawing of the length parameters that are relevant to an analysis of the fields in the prototype magnet.

	Parameter	Units	Value Inner, Outer
Coils	Number of cylinders		2
	Num of current blocks per cylinder		7,9
	Num of cable turns per layer		12, 12
	Num of layers per current block		9, 9
	Num of cable turns per block		108, 108
	Num of cable turns per cylinder		756, 972
	Total turns		1728
	Inner radius	mm	49.71, 68.63
	Outer radius	mm	60.02, 78.94
	Length, straight section	mm	1066.5
Length including ends	mm	1371.6	
Effective length, low field	mm	1203.5	
Effective length, high field	mm	1222.7	
Helix, length	mm	1200	
Helix, rotation	deg	180	
Helix, pitch	deg/mm	0.15	
Yoke	Inner radius in straight section	mm	84.46
	Outer radius	mm	177.80
	Length of lamination stack	mm	1029.1
	Inner radius at ends	mm	114.4
	Len of incr rad lam stack, ea end	mm	196.8
	Total length of lamination stack	mm	1422.8
Storage Unit	Weight	kg	795

Table 6.11: Selected mechanical parameters for the prototype slotted coil helical magnet. To optimize the design for single current operation, a layer of turns would be omitted from the pole-most current blocks in the inner and outer layers.

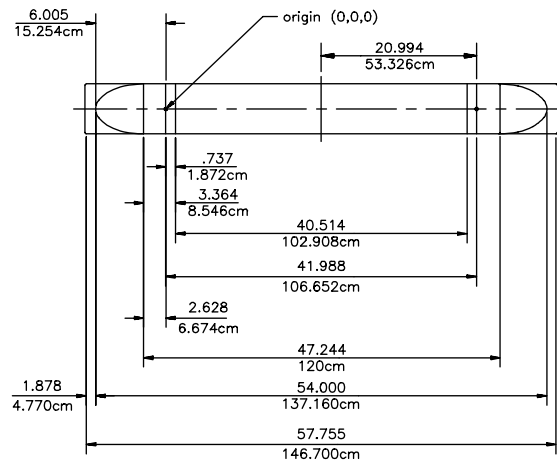


Figure 6.9: Length parameters of the prototype magnet. The inner and outer coils are the same in length. The ends begin at the point marked “origin.” The effective length was intended to be 1200 mm, with a total spiral rotation of 180° over that distance; the effective length achieved will be measured when the prototype is tested.

6.1.3 Electrical Design

The 16 separate windings of the two coils are connected in series at the end of the storage unit. These interconnections generate a small but manageable amount of heat. It is planned to connect a low-resistance resistor across each of the windings for quench protection. Without these resistors, a quench in a winding could absorb too much of the stored energy of the magnet and possibly lead to conductor damage. Resistors will provide a current bypass as coil resistance builds up following a quench. Since these magnets do not have a ramp rate requirement, resistors are the best choice — diodes could be used if there were a need to ramp the magnets during operation. The stored energy of the prototype magnet at 4 T is 120 kJ (1.2 m effective length) and the inductance is 2.4 H.

6.1.4 Quench Performance of Early Model

A model coil of an earlier design was built and tested in 1995. It reached short sample after a few training quenches, though the exact value was somewhat ambiguous because a good calculation of the peak field in the conductor was not available. That coil had 630 turns of the same cable in a similar configuration of windings in a slotted aluminum tube. The self inductance of that coil was 250 mH. The coil was instrumented with voltage taps and spot heaters for starting quenches at several selected locations. In the standard $\int I^2 dt$ language, it was found that 60 Kiits gave a hot spot temperature at high current of between

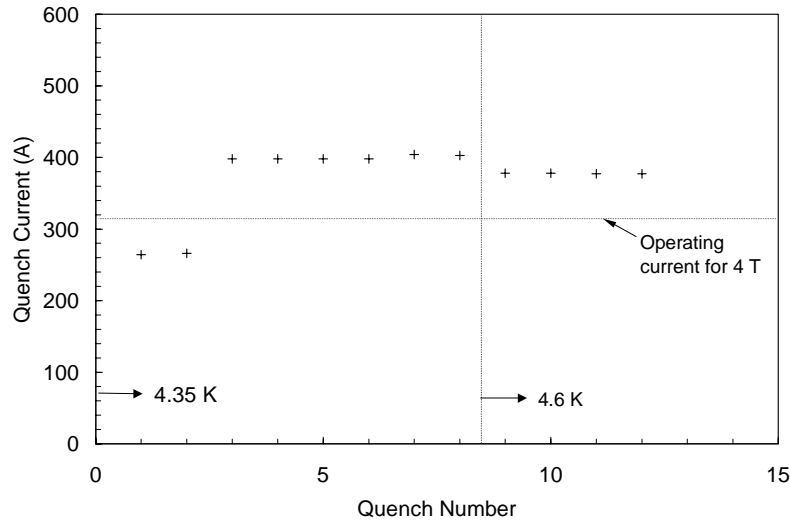


Figure 6.10: Quench performance of the prototype magnet. Following two low quenches, believed to have originated in the leads, the magnet quenched on a stable plateau following ramps at 0.1 A/s. Quenches 7 and 8 were slightly higher (6 A) because of the higher ramp rate used (1 A/s).

200 to 300°C, depending on whether the quench occurred in the pole winding (lower temperature) or the midplane winding. The maximum temperature recorded was for a midplane coil quench at 500 A: 490°C, 67 Kiits. These lower-than-calculated temperatures (calculations based on the amount of energy deposited in the windings) are the result of cooling from effects that are difficult to include in any calculation: effectiveness of cooling from helium, heat transfer to the surroundings, etc. Axial quench velocities in the windings were measured to be in the range 5-10 m/s for quenches with currents of 400-500 A. The short sample quench current for this coil was estimated at ~ 620 A.

6.2 Prototype Measurements and Final Magnet Design

A half-length, full field magnet using the design discussed in the previous section was built and tested at BNL. The magnet was powered and quench tested, including thermocycle testing, and detailed field measurements were performed using both Hall probes and rotating coils. The results of the field measurements and corresponding 3-D magnetic field calculations of the design have been used to generate a final specification for the body field rotation angle and to improve upon the design of the ends of the magnet.

6.2.1 Quench Results

The half-length prototype magnet built at Brookhaven in 1996, labeled HRC001, was tested in February 1997. Its quench performance was excellent, as shown in Fig. 6.10. After two low quenches, believed to

have originated in inadequately supported leads, the magnet quenched only at the level expected from prior tests on the cable. A shift in dewar temperature, and a variation in ramp rate, both moved the quench current in the expected direction — independent confirmation that the magnet was operating at the short sample limit. The current for all four quenches at the nominal test temperature (4.35 K) and ramp rate (0.1 A/s) was 398 A (4.8 T). At 4.6 K, the magnet quenched at 378 A. Not shown are several quenches with a dual current configuration powering the coils that reached 5.0 T, indicating that the design is not mechanically limited.

Examination of the voltage traces from each of the current blocks in the magnet indicates that during a spontaneous quench of the type recorded here (quench current at or near the short sample limit of the magnet), a quench beginning in one block is quickly followed (typically within 100 msec) by quenching in all the other blocks, presumably because of strong magnetic coupling due to the high mutual inductances of the windings. The voltage traces have been studied and reproduced using the program MicroCap V to model the magnet. The fast spread of the quench throughout the magnet is desirable for reducing the energy dissipated at the quench point. However, the quench propagation speed at lower currents is not known and needs to be studied in a magnet that can be intentionally quenched via spot heaters in the coils.

6.2.2 Harmonic Measurements

A 9 inch long rotating coil and a Hall probe system were used to make magnetic measurements. The 9 inch long rotating coil is considered the more reliable measuring system and its results are taken as the measured field values. A correction factor is applied to the measured harmonic values to correct for the decreasing sensitivity to higher harmonics as the field rotates over the coil's 9 inch length. This sensitivity is 98% for the dipole field component, 87% for the sextupole, 66% for the decapole, etc. The corrected, measured field values are shown in Fig. 6.11 (dipole field transfer function, in T/kA) and in Fig. 6.12 through Fig. 6.15 (multipole moments). In these figures, a multipole "unit" is the field value from that multipole relative to the central dipole field measured at the reference radius of the rotating coil (31 mm) times 10^4 .

Fig. 6.13 shows the measured sextupole field. At mid-range, the predicted value was -50.1 units for this harmonic, while the measured value is about -62 units. This is fairly good agreement considering the approximations involved in the calculations. The Hall probe system measured -76 units for the harmonic sextupole moment.

The Hall probe measurements have been more extensively analyzed and compared to a 3-D model calculation using TOSCA[48]. The z -dependence of the measurements and model results are in excellent agreement in the ends of the magnet, giving confidence that the calculation can be used to predict end behavior for changes in the design. The end design of the magnet is described in [49].

Because of the good quench performance of the prototype magnet, it is no longer necessary to consider

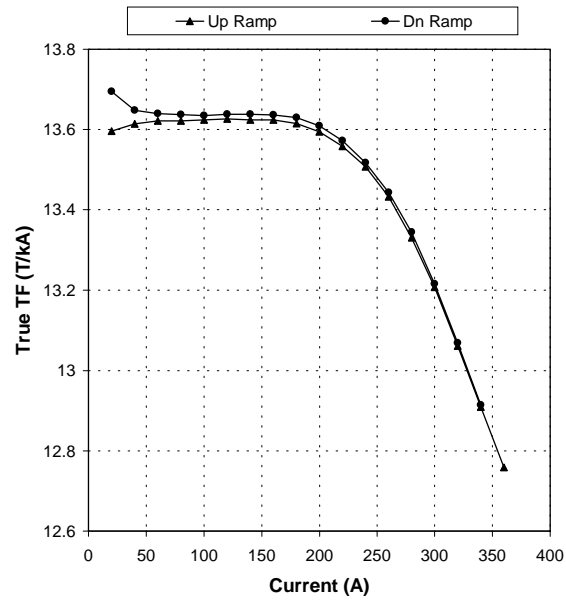


Figure 6.11: Measured dipole field transfer function for HRC001.

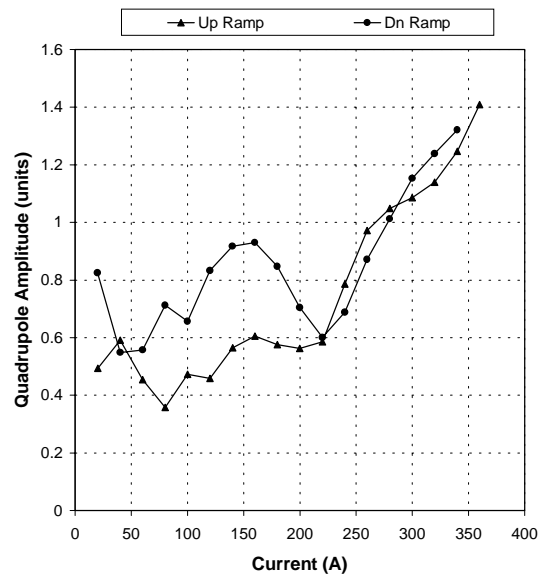


Figure 6.12: Measured quadrupole component for HRC001.

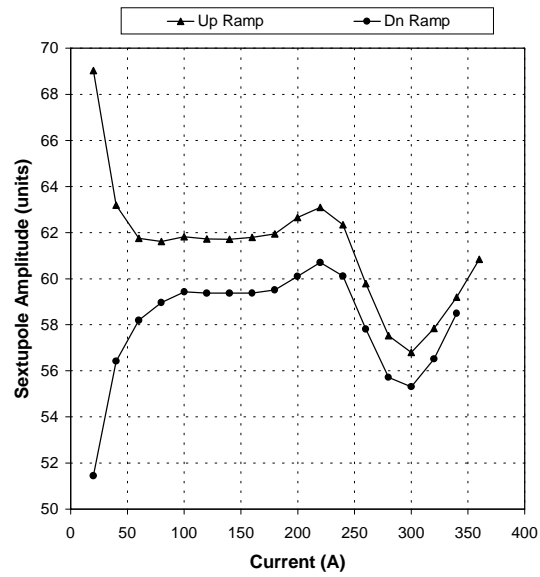


Figure 6.13: Measured sextupole component for HRC001.

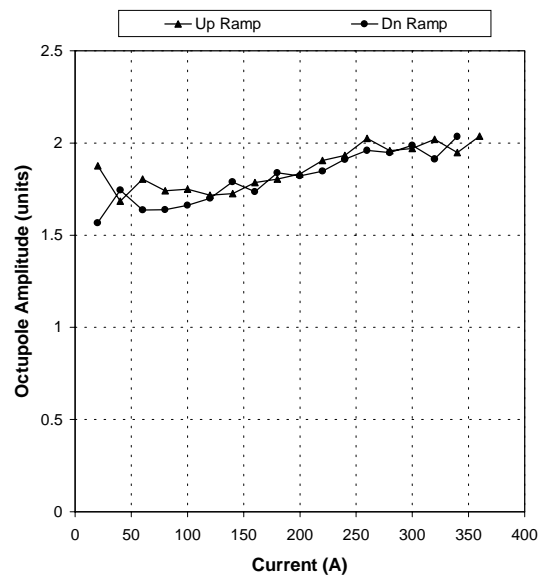


Figure 6.14: Measured octupole component for HRC001.

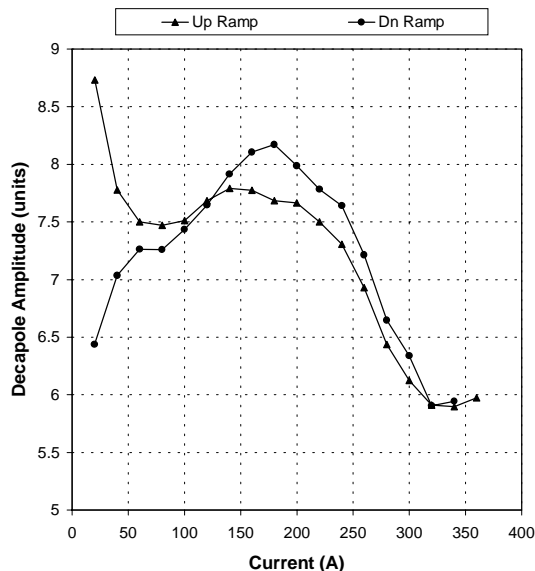


Figure 6.15: Measured decapole component for HRC001.

operation with dual currents to achieve adequate field margin. However, single current operation gives large harmonics. They could be reduced by relatively small changes in the current blocks. A suitable reduction is achieved by omitting a layer of turns in the pole-most blocks of both the inner and outer coils. With this change, the sextupole harmonic is predicted to be reduced to several units, with other harmonics also acceptably small. Future magnets will therefore be built with one less layer of turns (8 layers rather than 9) in the pole-most current blocks of both coils.

6.2.3 Rotation Angle

In the helical dipole magnets, the net deflection of the beam should be kept negligible.¹ In an oversimplified model, assuming a constant field strength over the magnetic length and zero field outside, the rotation angle of the field should be 360° . In practice, there are end regions where the field strength reduces gradually and the phase angle of the field changes very little. These end regions contribute to a net integrated dipole field, which must be compensated by an equal and opposite integrated dipole field from the body of the magnet. Due to lack of well defined boundaries, it is difficult to specify unambiguously a rotation angle. However, an effective rotation angle can be defined as the rotation angle in a simplified, “no ends” magnet, which will produce the same horizontal and vertical integrated dipole field as the real magnet. Thus, a magnet with zero integrated dipole field will be said to have an effective rotation angle of 360° .

If B_0 is the dipole field strength at the center of the magnet and θ_R is the effective rotation angle, then

¹NOTE: This section contains excerpts from [35], where additional information may be found.

the integrated y and x components of the dipole field in the transverse direction are given by

$$\int_{-\infty}^{\infty} B_y(z) dz = \left(\frac{2B_0}{d\alpha/dz} \right) \cos \left(\alpha_0 + \frac{\theta_R}{2} \right) \sin \left(\frac{\theta_R}{2} \right) \quad (6.1)$$

$$\int_{-\infty}^{\infty} B_x(z) dz = \left(\frac{2B_0}{d\alpha/dz} \right) \sin \left(\alpha_0 + \frac{\theta_R}{2} \right) \sin \left(\frac{\theta_R}{2} \right) \quad (6.2)$$

where $(d\alpha/dz)$ is the rate of change of phase angle in the body of the magnet. The quantity $(\alpha_0 + \theta_R/2)$ depends upon the choice of reference frame, and can be interpreted as the phase angle at the center of the magnet, assuming symmetric ends. It is easy to see that for a rotation angle of 360° the integrals of both the components vanish. One can eliminate the dependence on the reference frame by examining the total amplitude of the integrated field, C_1 , given by

$$C_1 = \left[\left(\int_{-\infty}^{\infty} B_y dz \right)^2 + \left(\int_{-\infty}^{\infty} B_x dz \right)^2 \right]^{1/2} = \left(\frac{2B_0}{d\alpha/dz} \right) \sin \left(\frac{\theta_R}{2} \right). \quad (6.3)$$

Using Eq. 6.3, one can estimate the effective rotation angle from the integrated dipole amplitude. It is clear from Eq. 6.3 that the integrated field is zero for a 360° rotation, and has a maximum for 180° . A consequence of this fact is that the integrated field is least sensitive to the rotation angle in a magnet with 180° rotation. A small error in the measurement of the integral field will result in a rather large error in estimating the effective rotation angle for such a magnet.

Using a rotating system consisting of two Hall probes, axial scans of the field in HRC001 were carried out at two currents — 105 A and 220 A. These currents correspond to approximately 1.43 and 3.0 Tesla respectively in the body of the magnet. For various reasons the data at 220 A are much more reliable for the purpose of estimating the integral field, and hence the effective rotation angle. Fig. 6.16 shows the measured dipole field amplitude and the phase angle as a function of axial position at 220 A, measured by the Hall probe-2, located at a radius of 3.56 cm. The Z -positions are from the reference point of the probe transporter, which is at an arbitrary position outside the magnet. Also, the Z -positions increase from the lead end to the non-lead end of the magnet, which is inconsistent with a right-handed coordinate system. The phase angle is in a reference frame decided by the orientation of the probe. This orientation is also arbitrary with respect to the yoke. The dipole amplitude and phase are obtained from a Fourier analysis of the measured radial component of the field at 64 angular positions. The measured data have been shown to agree very well with a three dimensional numerical calculation using TOSCA[34].

In principle, one could calculate the integral of the field components, B_x and B_y , from the data shown in Fig. 6.16. These integrated values can be used to obtain the total integrated dipole amplitude, C_1 , and the effective rotation angle, θ_R . Such a calculation yields a value of the integrated dipole amplitude of 2.286 T-m at a central field of 3.0083 T. The effective rotation angle calculated from this integrated field (see Eq. 6.3) is 173.8° . However, as pointed out above, the amplitude of the integrated field is not very sensitive to the effective rotation angle in a half-length magnet. Even small measurement errors could lead to very large error in the value of the effective rotation angle. For example, the integral dipole field

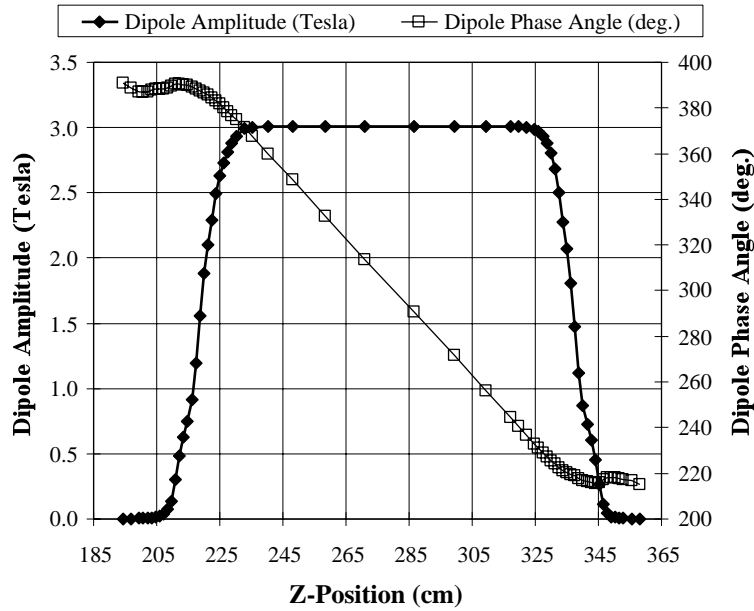


Figure 6.16: Measured dipole amplitude and phase at 220 A in HRC001.

expected for a 180° effective rotation angle instead of 173.8° is 2.289 T-m, which differs from the measured value by only 0.13%, well within the experimental errors.

A reasonable simulation of the actual full length magnet can be made by assuming that the ends of the magnet are identical to those in HRC001, but the straight section is longer by one half-period. The “experimental” data in such a full length magnet can be generated by dividing the actual data in HRC001 into two halves at any location in the body of the magnet, and then sandwiching a straight section with a uniform rate of twist and a constant dipole field amplitude between the two halves. The field amplitude of this extra section is given by the average amplitude over the central region of the prototype HRC001. The phase angle at various points in this region can be calculated from the nearest data point in HRC001 and the known rate of twist. With this extra half length sandwiched between the two halves of the measured data, the phase angles of the second half will be shifted by 180° from the actually measured values and the Z -positions will change by half a wavelength. In this way, one can generate a very good approximation to the experimental data that would have been recorded, had the magnet been of a full length.

Fig. 6.17 shows the simulated data at 220 A for a full length magnet, generated by a procedure as described above. In order to be consistent with the reference frame used in numerical simulations, the origin in the experimental data has been shifted to bring the magnet center at $Z = 0$. Also, the reference frame is rotated to make the integrated B_x component zero. Furthermore, the Z -axis is inverted to make the coordinate system right-handed. The two transverse components of the dipole field are shown in

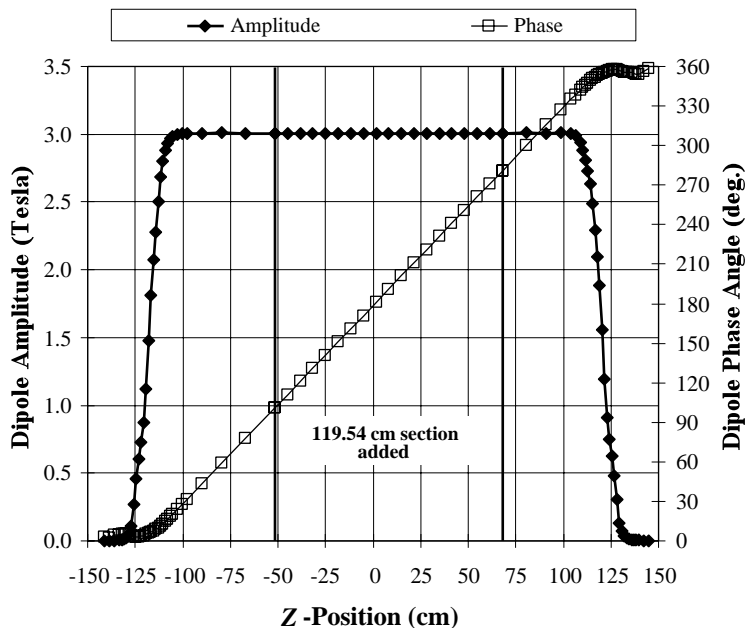


Figure 6.17: Simulated data at 220 A in a full length helical magnet. The Z -axis is inverted from the raw data in Fig. 6.16 to obtain a right handed coordinate system.

Fig. 6.18. It is seen that with this choice of reference frame, the dipole field is in the positive y -direction near the ends of the magnet ($\alpha_0 \approx 0$ in Eqs. 6.1 and 6.2). The length of the section added is 1.2 m at room temperature, or 1.1954 m at liquid helium temperature. A twist rate of 1.5057 degrees/cm gives a rotation of exactly 180° over this extra section.

The values of $\int B_y(z)dz$ and $\int B_z(z)dz$ are obtained by numerically integrating the data in Fig. 6.18. This integration was carried out in three separate regions — the two “end” regions made up of two halves of the actually measured data, and the “central” region consisting of the additional half length in the middle of the magnet. The integrated field in the “central” region can also be calculated analytically using Eqs. 6.1 and 6.2. The analytical result was used to check the accuracy of the numerical integration procedure. Since the measured data points are at non-uniform Z -intervals, it was convenient to use a piecewise linear approximation to the actual curve. Since the final result of integration is expected to be a small number, even small errors in integration can lead to large errors. Based on a comparison with the analytical value in the central region, a linear approximation between data points was found to be unsatisfactory. A 3-point integration formula for arbitrary increments was developed for a more precise integration. If the three distinct points are given by x_1 , x_2 , and x_3 , then the integration of any function from x_1 to x_3 can be shown to be given by

$$\int_{x_1}^{x_3} f(x)dx \approx a_1 f(x_1) + a_2 f(x_2) + a_3 f(x_3) \quad (6.4)$$

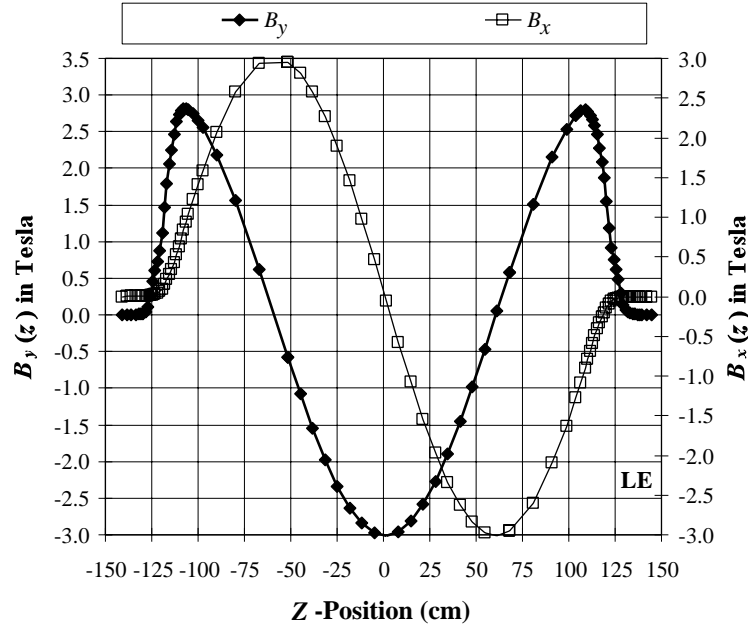


Figure 6.18: Simulated data for $B_x(z)$ and $B_y(z)$ at 220 A in a full length helical magnet.

where

$$a_1 = \frac{(x_3 - x_1)}{6(x_2 - x_1)} [2(x_2 - x_1) - (x_3 - x_2)] \quad (6.5)$$

$$a_2 = \frac{(x_3 - x_1)^3}{6(x_2 - x_1)(x_3 - x_2)} \quad (6.6)$$

$$a_3 = \frac{(x_3 - x_1)}{6(x_3 - x_2)} [2(x_3 - x_2) - (x_2 - x_1)] \quad (6.7)$$

Eq. 6.4 gives an exact integration for functions up to second order in x . This integration formula gave the correct integral field for the central region. The end regions were integrated numerically using Eq. 6.4, but the analytical value was used for the central region, even though a numerical integration also gave the same result.

The results of the calculations are summarized in Table 6.12. The integration of simulated data in Fig. 6.18, as described above, gave an integrated dipole field, C_1 , of 193.96 Gauss-m at a central field of 3 T, corresponding to an effective rotation angle of $\theta_R = 360.97^\circ$. It should be recalled that the integrated x -component is made zero by an arbitrary choice of reference frame. It is interesting to estimate the uncertainty in the calculated value of the effective rotation angle. Assuming a $\pm 0.2\%$ error in the calculation of the integrated field strength (base on the 0.13% discrepancy seen in the half length magnet data), the maximum error in the effective rotation angle is only $\pm 0.002^\circ$. Even if a rather large error of $\pm 10\%$ in the integral field is assumed, the error in the calculation of the effective rotation angle is only

Current (A)	Hall Probe	Central Field B_0 (T)	$\int B_y(z)dz$ Gauss-m	$\int B_x(z)dz$ Gauss-m	Integrated dipole Ampl. C_1 (Gauss-m)	Rotation Angle θ_R (deg.)
220	1	3.007	208.06	0.00	208.06	361.04
220	2	3.008	193.96	0.00	193.96	360.97

Table 6.12: Summary of rotation angles calculated for a full length magnet.

$\pm 0.10^\circ$. This is in sharp contrast with the case of the half-length magnet where even a 0.1% uncertainty leads to an error of several degrees.

Even though the data at 105 A had problems, an analysis was nevertheless performed to obtain the effective rotation angle at this current as well. A value of 360.98° was obtained with the data from either of the two probes. These values are consistent with those obtained at 220 A.

A full three dimensional analysis of the field in the helical magnet has been carried out to optimize the rotation angle[50]. This analysis suggests that the effective rotation angle of the full length magnet with the present end design should be about 360.75° , which is close to the 360.97° estimated above from the simulated data. The value of 194 Gauss-m for the integral field at a central field of 3.0 T is well within the tolerance of 500 Gauss-m at 4.0 T[33]. Based upon the present analysis, no change in the length of the production magnets is necessary.

6.2.4 Modification of End Design

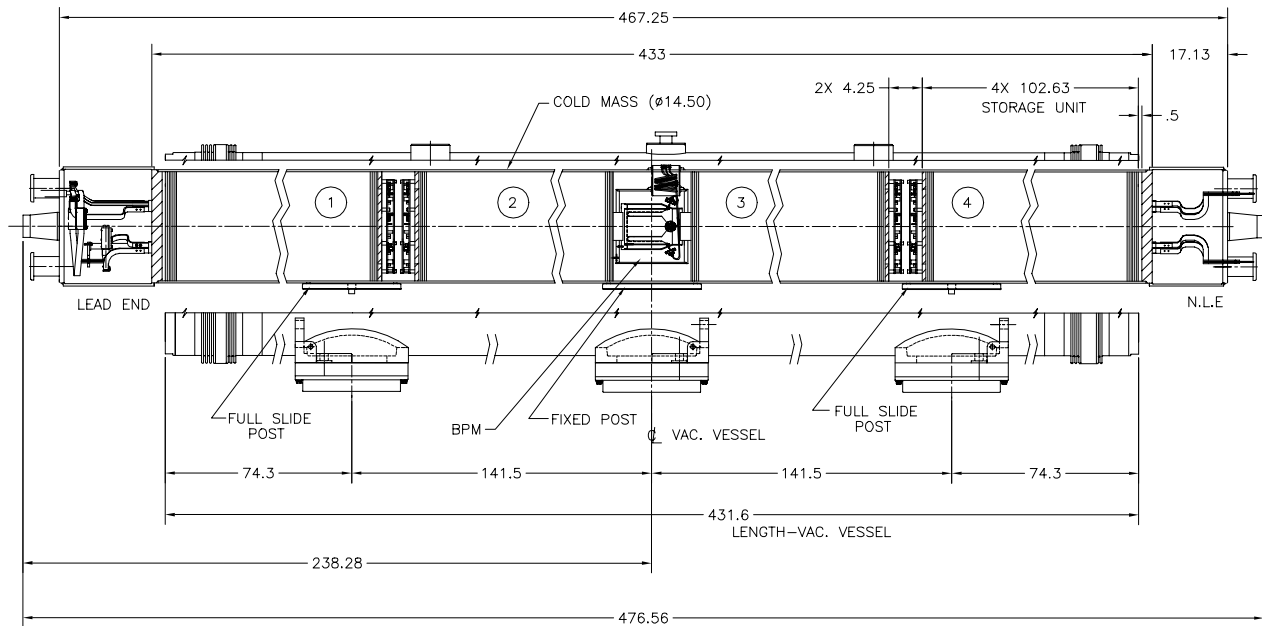
The ends of the magnet HRC001 had several current blocks where the wall between adjacent blocks was rather narrow. To ease problems in construction with these narrow walls, they will be widened in subsequent models. This design change has been modeled and the preliminary analysis shows that the effective rotation angle in the as-built full length magnet will be smaller by at least 0.25° [34]. This should significantly reduce the value of the integrated dipole field from the present estimate.

6.3 Snake and Rotator Assemblies

Each Snake and Rotator will be comprised of four superconducting helical dipole magnets making up a single cryostat assembly. With the Snake assemblies being located in the cold straight section between RHIC quadrupoles Q7 and Q8 (see Section 6.1), the cryostat for this assembly will be a modified “DU7” cryostat nominally used at these locations. The length of this cryostat (with the new nomenclature “DU3”) is 11.876 m, slightly longer than a typical RHIC dipole magnet. This is due to the fact that the Q7 quadrupole, in the transition region between the arc and interaction region lattices, is slightly shorter than typical RHIC arc quadrupoles. Though the Rotators are located at the ends of a 30 m warm straight section, these assemblies will also reside in DU3 cryostats in order to make more efficient use of cryostat

hardware. A sketch of the cold mass assembly within a DU3 cryostat is shown in Fig. 6.19 for the Snakes and Fig. 6.20 for the Spin Rotators. Specifications for magnet placement and alignment were provided in Table 6.3.

1. MODEL - 01, YELLOW RING WITH MODEL 01 COLD MASS.
2. MODEL - 02, BLUE RING WITH MODEL 01 COLD MASS.



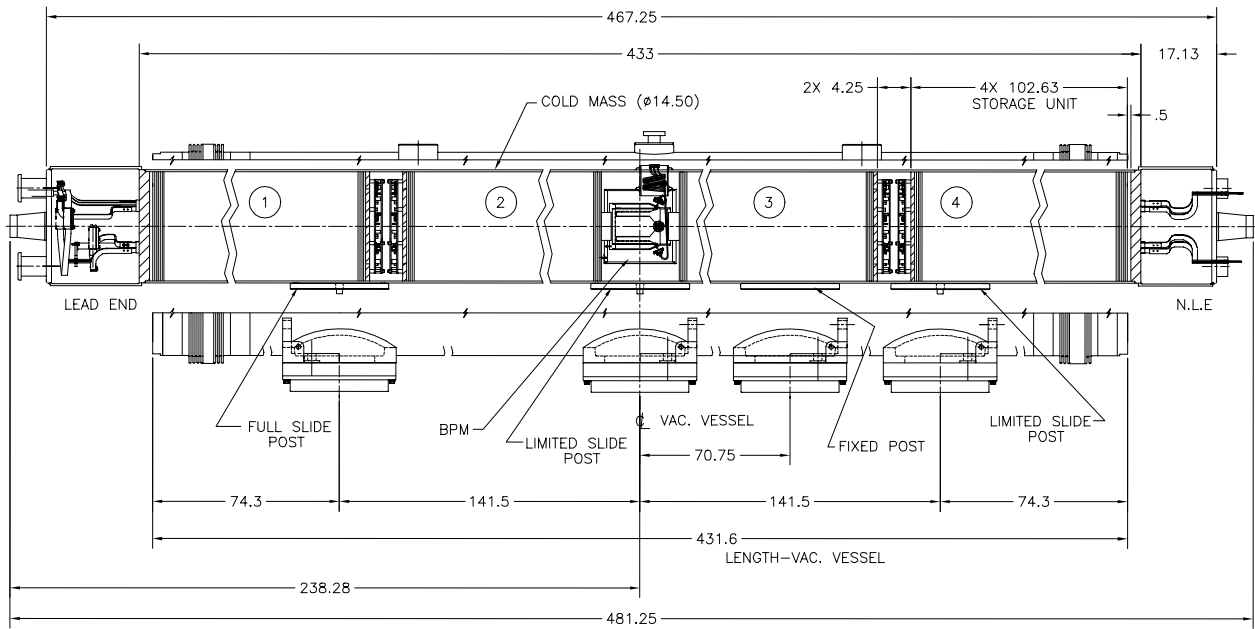
HELICAL DIPOLE MAGNET
DIMENSIONAL DRAWING
"SNAKE"

Figure 6.19: Sketch of Snake cryostat assembly. The four superconducting helical dipole magnets are located within a common cryostat. A dual-plane BPM is located near the center of the assembly.

6.3.1 Snake/Rotator Coldmass

Four individual helical cold masses, or "storage units," each ~ 2.4 m long, are assembled into a single cold mass ~ 10 m long. This is done by welding a stainless steel shell around the storage units as they are positioned on a fixture that gives accurate alignment of the units relative to one another. The beam position monitor that is required in the middle of this coldmass and the various electrical interconnections that must be made are completed before the shells are positioned. After the cylindrical shells are welded in

1. MODEL - 03, YELLOW RING WITH MODEL 03 COLD MASS.
2. MODEL - 04, BLUE RING WITH MODEL 02 COLD MASS.
3. MODEL - 05, BLUE RING WITH MODEL 03 COLD MASS.
4. MODEL - 06, YELLOW RING WITH MODEL 02 COLD MASS.



HELICAL DIPOLE MAGNET
DIMENSIONAL DRAWING
"SPIN ROTATOR"

Figure 6.20: Sketch of Rotator cryostat assembly. This assembly, at the end of a cryo string, has different support post requirements than the Snakes.

place, end plates are welded to either end to terminate and align the assembly. The beam tube is welded to the end plates in order to enclose the helium volume. Its diameter increases from the nominal 7.30 cm diameter used in the RHIC arcs to the larger 9.05 cm diameter used in the helical magnets through a short cone-shaped transition piece, 8.89 cm long, at each end of the assembly.

A partial drawing of this assembly is shown in Fig. 6.21. Not shown are fiducial targets that reference the units to the outside.

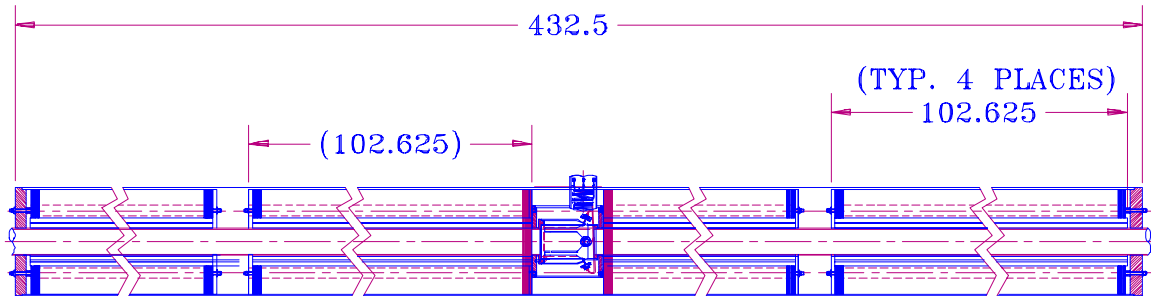


Figure 6.21: A Snake or Rotator cold mass consists of four individual helical cold masses, or “storage units,” assembled into an integrated assembly as shown. Dimensions are shown in inches.

Before the coldmass can be installed into a cryostat, the electrical interconnects including bus expansion loops must be assembled in the ends. Busses to carry current for the RHIC arc magnet system must be installed through the slots that have been provided in the storage units. Finally, the ends are closed and made helium-tight with cylindrical containments welded to the end plates and terminating in the appropriate joints for interconnecting to the adjacent arc system. Power for the helical magnets is provided locally at each Snake or Rotator position through current feedthroughs that are welded to the shell in two locations along its length.

6.3.2 Cryostat Assembly

The coldmass is finally installed into a cryostat consisting of a vacuum tank, heat shield, and piping to carry the cryogens. Plastic posts similar to those used for the magnets in RHIC support the coldmass in three places and are designed to allow thermal motion with one anchor point. The vacuum tank is somewhat larger (~ 50 mm) than the standard 610 mm tank used in RHIC in order to accommodate the larger diameter helical coldmass. Legs on the vacuum tank in two places support the assembly on stands in the tunnel. The cryogenic piping is necessarily somewhat rearranged with respect to the standard RHIC

layout so that adapters are needed to connect the helical assembly to the neighboring magnets in RHIC. A cross section view of the cryostat assembly is shown in Fig. 6.22.

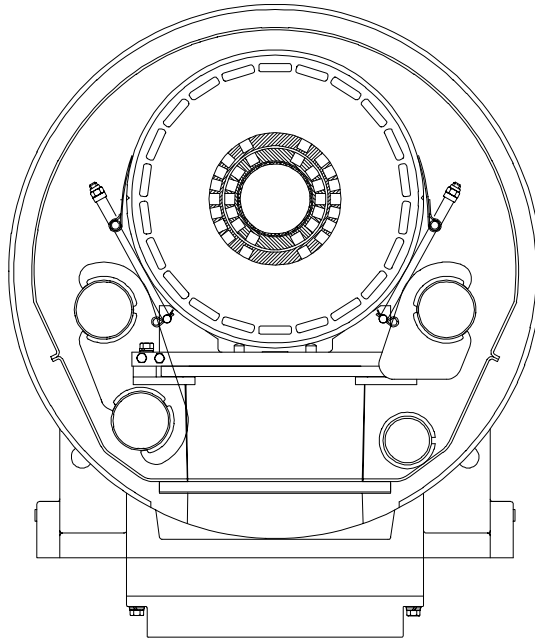


Figure 6.22: Helical magnet assembly in its cryostat. The outside diameter of the vacuum tank is 660 mm.

As seen in Figs. 6.19 and 6.20, some extra room is located between superconducting magnets at the center of the Snakes and Rotators for the internal Beam Position Monitor. Tolerances for the BPM alignment are indicated in Table 6.13. The layout of the internal BPM is sketched in Fig. 6.23.

Parameter	Requirement	Tolerance (rms)
Number of BPMs (each, hor. & ver.)	12	
BPM Transverse Alignment	0 mm	5 mm
BPM Longitudinal Alignment	0 mm	5 mm
BPM Rotational Alignment	0 mrad	25 mrad

Table 6.13: BPM position tolerances with respect to neighboring quadrupoles.

The internal BPMs will be a modified version of the RHIC triplet BPMs [51],[52]. The 11.2 cm aperture dual-plane detectors will be 13 cm long short-circuited 50 ohm strip transmission lines subtending 70

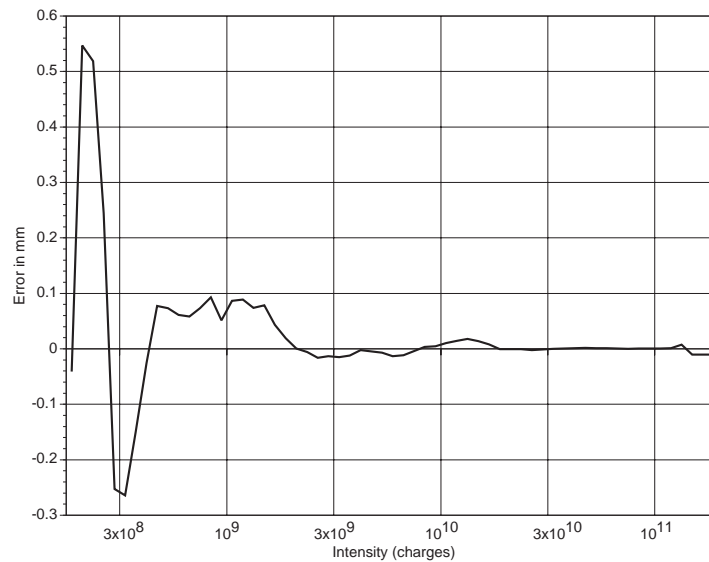


Figure 6.24: Measurement error of the internal BPM, assuming the beam is located near the center of the device. For expected large beam offsets, the error will be worse by roughly one order of magnitude.

This non-linearity may be corrected by digital processing [56], using the mapped response of the BPM.

The primary limitation on the electronic accuracy of the position measurement is the linearity of the track and hold modules. As the beam moves off center the difference between the outputs of the opposing striplines increases, resulting in an increase in the effect of this non-linearity. Fig. 6.24 shows the result of a calculation of the effect of track and hold non-linearity for normal RHIC operating conditions [52]. The increase in error is approximately linear with offset, and for a 4 cm offset the error should be about an order of magnitude greater than that shown in the figure.

The primary limitation on resolution is noise injected in the track and hold modules. The BPM electronics performs a “difference over sum” measurement. As the beam moves off center the power to the more distant electrode is reduced, reducing the signal-to-noise ratio. Fig 6.25 shows the result of a calculation of the effect of noise on position measurement resolution for normal RHIC operating conditions [52]. The decrease in resolution is approximately linear with offset, and for 4 cm offset the resolution should be less than one order of magnitude worse than that shown in the figure.

If greater accuracy and resolution is required, the width of the input filter passband might be reduced. This would eliminate the possibility of measuring beam position on a bunch-by-bunch basis, but would result in considerable improvement in accuracy and resolution. In addition, there is also the possibility of calibrating a complete system of BPM plus electronics using the BPM mapping facility [51], and using this calibration in the digital processing.

The magnitude of the peak voltages and currents seen by the feedthroughs, signal cables, and electronics is affected by bunch length and by beam intensity and position. With possible future upgrade beam

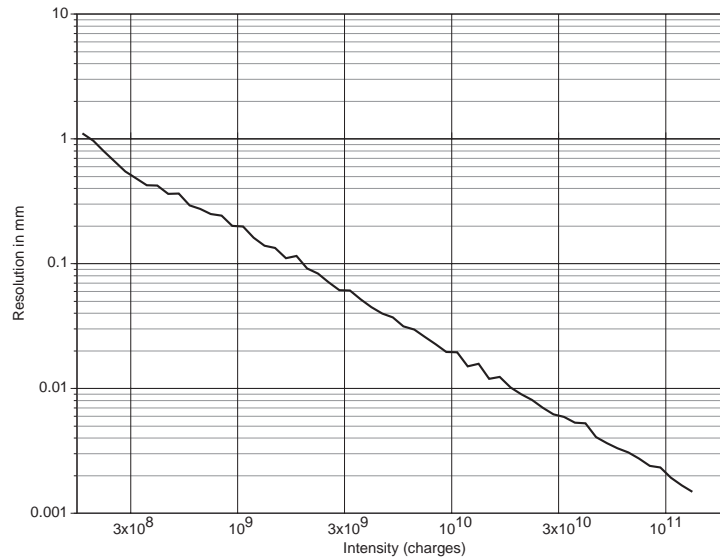


Figure 6.25: Position resolution of the internal BPM, assuming the beam is located near the center of the device. For expected large beam offsets, the resolution will be worse by less than one order of magnitude.

intensity of 2.5×10^{11} protons per bunch, and an rms bunch length of 15 cm, the maximum signal voltage will be in the range of 500 to 600 volts. This will require attenuation at the cryostat. Heating of the cryogenic signal cables within the cryostat will require that they be properly thermally anchored. Heating of the cable, and the corresponding variations in insertion loss resulting from the temperature dependent resistivity of the cable, can be compensated in the digital processing if necessary. With its large beam offsets the snake BPM might be a useful test platform for exploring the effects of signal cable heating in more detail.

6.4 Other Accelerator Systems Hardware

6.4.1 Power Supplies and Controls

The slotted helical dipole magnet design requires about 320 Amp for 4 Tesla operation. The power supplies for these magnets do not require many special features. The Snake magnets are run DC and at constant current throughout the acceleration cycle. The Rotator magnet settings are energy dependent, but the Rotators are not required to be on until the beams are in collision. It will be important for the Rotator magnet power supplies to be able to track each other when they are turned on, but because this is an adiabatic operation the ramp will be purposefully slow and the tracking requirements are very lenient. Standard RHIC control devices will enable all standard Snake and Rotator power supply operations.

While the RHIC Spin system will introduce 24 new Beam Position Monitors (12 units with both horizontal and vertical position readout) to the RHIC ring, this will be a small perturbation to the RHIC

Parameter	Requirement	Tolerance (rms)
Power Supply Current (I)	320 A	
Current Setting/Adjustment ($\delta I/I$)	0.5%	
Current Regulation/Stability ($\Delta I/I$)	0	0.01%
Ramp rate (dI/dt) (Rotator only)	1 A/sec	0.01 A/sec

Table 6.14: Snake/Rotator Power Supply requirements.

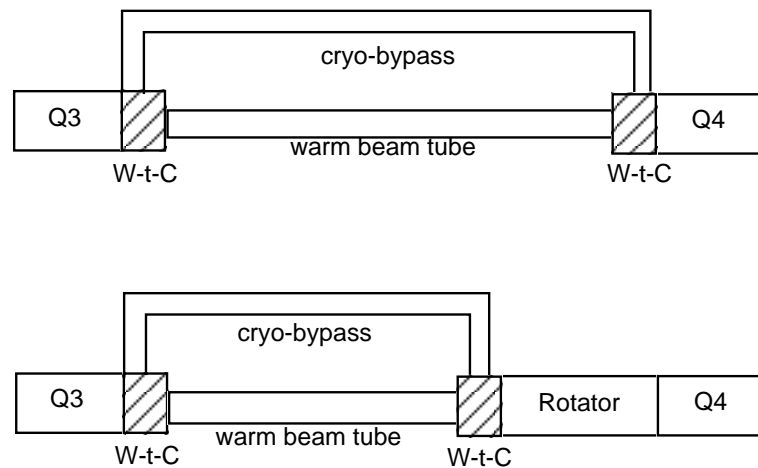


Figure 6.26: Sketch of cryo system modifications required at the Rotator locations in the RHIC tunnel.

BPM system which already has nearly 500 such devices. Standard RHIC signal processing and controls hardware will be employed in the Snake/Rotator BPM system.

6.4.2 RHIC Vacuum and Cryogenics Interface

The Snake and Rotator assemblies are contained within RHIC dipole-style cryostats with standard magnet interconnections to adjoining cryogenic devices. The one major change in the RHIC vacuum and cryogenics system which is to be incorporated as a consequence of the Spin system is at the Rotator locations. The Rotators reside in the warm straight sections between quadrupoles Q3 and Q4, immediately next to Q3. Thus, the length of the actual warm beam pipe at these locations and the associated cryogenics bypass need to be shortened. These modifications are indicated in Fig. 6.26. The modifications include shortening of the warm beam tube and of the cryogenic bypass assembly, while the end boxes and end connections remain standard.

